IEEE Access
Multidisciplinary | Rapid Review | Open Access Journal

Received 29 May 2022, accepted 16 June 2022, date of publication 21 June 2022, date of current version 27 June 2022.

Digital Object Identifier 10.1109/ACCESS.2022.3185056

Inertia Assessment From Transient Measurements: Recent Perspective From Japanese WAMS

THONGCHART KERDPHOL[1], (Member, IEEE), MASAYUKI WATANABE[1], (Member, IEEE), YASUNORI MITANI[1], (Member, IEEE), AND ISSARACHAI NGAMROO[2], (Senior Member, IEEE)

[1]Department of Electrical and Electronic Engineering, Kyushu Institute of Technology, Kitakyushu 804-8550, Japan
[2]Department of Electrical Engineering, Faculty of Engineering, King Mongkut's Institute of Technology Ladkrabang, Bangkok 10520, Thailand

Corresponding author: Issarachai Ngamroo (issarachai.ng@kmitl.ac.th)

This work was supported in part by the New Energy and Industrial Technology Development Organization (NEDO), Japan, under Grant JPNP19002; and in part by the National Research Council of Thailand.

ABSTRACT Currently, the substantial renewable penetration brings a low inertia issue to the Japanese power system, threatening stability and resiliency than ever. The inertia estimation based on transient events provides a reliable basis for system control and operation. However, the poor rate of change of frequency extraction from different types and locations of phasor measurement units (PMUs) could significantly lead to inertia estimation errors. As a remedy with a lesson learned, this paper analyzes effective inertia estimations based on transient measurements of the Japanese wide-area monitoring in both distribution and transmission levels. Due to the longitudinally interconnected configuration of the 60 Hz Japanese power system, the polynomial approximation technique is proposed to restrain the strong effect of oscillatory components. To enhance the estimation performance considering an existing center of inertia, the comprehensive mode-shape analysis is performed via geographical measurement locations, indicating sufficient PMUs with precise estimation. The effectiveness of inertia estimation techniques is verified through actual system events corresponding to various transient sites. The numerical results demonstrate that recent inertia of the 60 Hz Japanese system with existing renewables ranges around 7.12 - 8.13 s in its system load base.

INDEX TERMS Inertia estimation, power system dynamics, synchrophasor measurement, transient response, wide-area monitoring.

I. INTRODUCTION

Inertia is considered as an inherent physical property of power systems, which has a major influence on system dynamics. Following an important transient/disturbance event (e.g., power unbalance, load/generation loss), the deviation of system frequency relies on valid quantities of kinetic energy accumulated in the generator's rotating mass [1]. The kinetic energy is characterized by the inertia of spinning generators in a system, which is the key function in calculating the initial frequency response after the disturbance. If the system inertia becomes vastly uncertain, the frequency deviation will considerably become volatile, potentially leading to cascading failures. Hence, the system inertia offers abrupt power when necessary, maintaining the stable system for any credible disturbances [2].

With the increasing concerns of climate change and global warming, a substantial portion of renewable energy sources (RESs) and high capacity of interconnected systems are being integrated into today's power systems. Most of RESs are connected to power systems via the interfaces of power electronics (i.e., inverters/converters) and provide minimal to no inertia properties [3]. As a result, the increasing share of RESs significantly decreases the available level of system inertia, causing the system to be more sensitive to frequency stability problems [4], [5]. Accordingly, the situations of low system inertia result in the rapid rate of change of frequency (RoCoF) and higher frequency deviations (e.g., nadir and overshoot), causing the tripping of protection relays and generators. Such conditions could undermine the control

The associate editor coordinating the review of this manuscript and approving it for publication was Hassen Ouakad.

and protection schemes of the system and even cause a widespread interruption or complete power blackout [6], [7].

The advent of synchronized measurement technology such as phasor measurement units (PMUs) has led to the quick expansion of a wide-area monitoring system (WAMS) [2], [8]. The installation of WAMS in the form of PMUs introduces the new possibility of acquiring measurement data in an accurate (synchronized) way via several points of the network. Consequently, the quantity of accessible measurement data is raised. Moreover, monitoring area (local) frequency enables PMUs to be efficiently exploited, creating a real-time WAMS in the presence of disturbances [9]. Thus, the PMUs-based system inertia estimation becomes possible. The inertia estimation approves the transmission system operators (TSOs) to identify the inertia level of a system so that sufficient power reserves are retained, avoiding the potential risk of instability. In the past, the inertia quantities of real-world power systems (i.e., the Nordic system [10], the Western Electricity Coordination Council system [11], and the 60 Hz Japanese system [12]) were determined without considering the PMUs and RESs integration. By enabling the PMUs, the inertia quantities of the Great Britain [13] and Iranian systems [14] were determined under the impact of RESs penetration.

With the rising levels of RESs, the importance of inertia estimation is boosting attention from various TSOs. Until now, the swing equation-based two estimation techniques are used for successful inertia calculation. The first estimation method calculated the inertia based on the operation of large disturbance/transient events (e.g., generation/load [2], [9]–[19]. Another estimation method calculated the inertia based on the steady-state operation (e.g., small-signal events) [6], [20]–[23]. In this paper, we have focused on the inertia estimation method based on transient events. For the successful operation, one of the major criteria is characterized by calculating the frequency and RoCoF. Previously, the measured frequency from a generator was used to calculate the RoCoF [10]. Later, this technique was expanded to measure the average frequencies for all generators. Afterward, this technique was adjusted to measure the averaged frequency of area generators for the calculation [16], [24]. Accordingly, the capability of estimating system inertia becomes feasible.

Another key challenge relies on the accurate latency of inertia estimation, which is affected by the oscillatory components during the transient event. The measurement data obtained by PMUs include several oscillatory components associated with local oscillations, interarea oscillations, and noises. The frequency and RoCoF calculations may be prone to accuracy issues. Such influences will be exacerbated in the longitudinal transmission network, which can critically lead to a huge error in inertia estimation. Without accurate inertia estimation, the TSOs cannot take corrective actions to retain power reserves and maintain system stability during the disturbance [25].

The effective solution for accommodating large oscillatory components was introduced in [12] using the polynomial approximation technique. The approach was extended to examine the inertia of the Taiwanese power system [26]. The results confirmed that the polynomial approximation could substantially diminish the inertia estimation error. However, the mentioned references did not investigate the PMU types and geographical locations concerning the center of inertia (COI) motion, which may affect the polynomial approximation-based inertia estimation performance. In real practice, these factors can lead to a potential inertia estimation error. To fill in this research gap, this paper examines the polynomial approximation technique considering the significant influences of various PMU types, PMU locations, transient sizes, and transient locations. With the increasing RESs penetration throughout Japan, this work also aims to determine the updated inertia of the 60 Hz Japanese system with substantial RESs via the recorded transient events. In this study, distribution-level PMUs (μPMUs) and transmission-level PMUs installed along with the longitudinal (wide-area) network have been investigated to collect the high-resolution phasor data for frequency calculation. Later, the equivalent swing equation is utilized for successful inertia estimation. Instead of calculating the RoCoF, the fifth-order polynomial coefficient is evaluated based on the change of frequency with respect to time, improving the accuracy of inertia estimation. Considering the influence of interarea oscillations throughout various PMU locations in the wide-area system, the mode shape analysis is used to determine an effective PMU-based COI for guaranteeing accurate inertia estimation. The results are compared with the conventional inertia estimation-based RoCoF calculation [16] and the known contribution of measurable system inertia from online synchronous generations [27].

The main contributions of this research over the PMU-based inertia estimation approaches are emphasized as:

i) This paper evaluates the effective inertia estimation of a real-world power system (i.e., the 60 Hz Japanese system) considering the dynamic influences of existing PMU types (i.e., μPMUs from the campus WAMS and transmission-PMUs from the TSO-WAMS) and potential PMU locations in respect to real transient sizes and locations. The real measurement data used in this analysis are included the effects of RESs penetration (i.e., photovoltaic and wind turbine systems) in the 60 Hz system. Using the proposed polynomial approximation technique, a changing order of polynomial approximation is performed over the measured frequency from μPMUs and transmission-PMUs, which significantly reduces the inertia estimation error and helps to restrain the influence of large oscillatory components and transients/disturbances from the longitudinally interconnected system.
ii) Most of the reports on inertia estimation based on transient events are mainly concentrated on rural power systems where no RESs or small size of RESs is contained, and frequency transients can be

directly analyzed without considering the characteristic of oscillatory components, causing inertia estimation errors. On the contrary, this research analyzed the inertia estimation based on a realistic interconnected system with a substantial RES penetration, where the influence of oscillatory components with respect to the transient calculation is suitably arrested, resulting in the accurate latency of inertia estimation.

iii) As a result, this paper reveals a practical lesson learned with a potential solution, which is favorable for enhancing a wide range of diagnostic and control functionality of inertia estimation based on transient events for a longitudinally interconnected system with substantial RESs integration.

The remainder of this work is arranged as follows: Section II explains the fundamental theory regarding system inertia estimation. Section III describes a practical structure of Japanese WAMS for inertia estimation. Section IV proposes the design of the polynomial approximation technique corresponding to PMUs measurement to accommodate the oscillatory components for transient-based inertia estimation. Section V shows the results of PMUs-based inertia estimation. Section VI demonstrates a practical technique to qualify an effective PMU location for guaranteeing accurate inertia estimation. Finally, conclusions are given in Section VII.

II. FUNDAMENTAL THEORY INERTIA PROPERTY

A. INERTIA PROPERTY

The inertia property indicates a certain amount of kinetic energy accumulated in a rotor of spinning/synchronous generators linked to the system. The inertia amount indicates the time for the total energy accumulation in all rotors, which is used for supporting the entire rated power during a disturbance. The accumulated kinetic energy could be divided by the rotational speed and moment of inertia. When the accumulated energy is divided by the rated power, the inertia of a rotor can be evaluated, and such quantity continually variates. Normally, it is presumed that the rotor runs at its rated speed. Accordingly, the assumed rule reformulates the inertia into the specific term of inertia constant (H) with the unit of second (s) [2], [13]:

$$H = \frac{J\omega_r^2}{2S_r} \tag{1}$$

where J is the inertia moment of a rotor (kgm^2), ω_r is the rated speed (rad/s), and S_r is the rated power (W).

B. SWING EQUATION-BASED INERTIA ESTIMATION

After a large disturbance/transient, the initial frequency response is usually governed using the inertia property. With approximation, the entire system can be characterized by the equivalent single generator. Thus, the equivalent swing equation can be used for a control system or area. Following a disturbance in area j, the swing equation-based frequency deviation can be written in the form of angular momentum

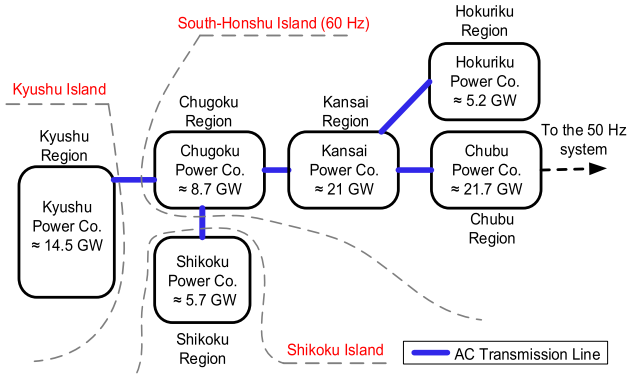

FIGURE 1. Overview of the 60 Hz Japanese power system with interconnections.

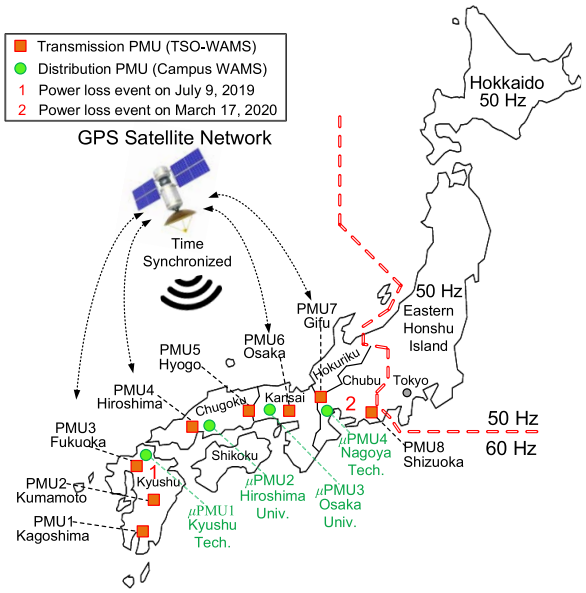

FIGURE 2. Configuration of the 60 Hz Japanese WAMS for inertia estimation.

(M_j) as [6], [12], [15]:

$$\omega_j \left(M_j - \Delta M_j\right) = \frac{\Delta P_j}{\frac{d(f_j/f_{sj})}{dt}} \tag{2}$$

$$M_j = \frac{\Delta P_j}{\omega_j \left(\frac{d(f_j/f_{sj})}{dt}\right)} + \Delta M_j \tag{3}$$

where M_j is outlined in terms of frequency as $M_j = 2H_jS_j$, ΔM_j is the variation in inertia energy triggered by a transient event, ΔP_j is the change in active power caused by a transient event, H_j is the inertia constant, S_j is the entire generated power, ω_j is the rated speed ($\omega_j = 2\pi f_{sj}$), f_j is the frequency, f_{sj} is the rated steady-state frequency, and df_j/dt is the RoCoF.

Subsequently, if system frequency and power data during the disturbance are suitably measured, (2) can be used to determine the whole system inertia.

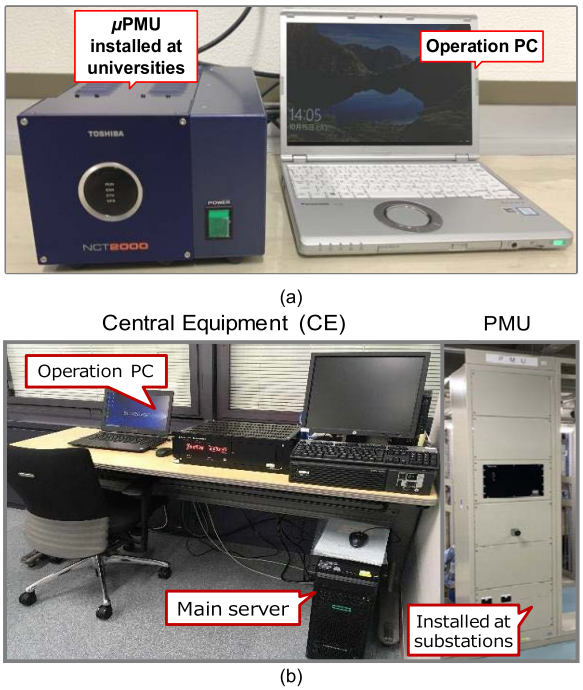

FIGURE 3. Collection of phasor data for inertia estimation: (a) distribution-PMU system; (b) transmission-PMU system.

III. CONFIGURATION OF THE 60 Hz JAPANESE WAMS

Due to antiquity, the Japanese power grid is separated into two frequency operations. The eastern territory (from Hokkaido Island to Tokyo prefecture) is operating at 50 Hz, while the western territory (from Shizuoka prefecture to Kyushu Island) is operating at 60 Hz. Three AC/DC converters are used to link both systems. The 60 Hz system contains a longitudinal (wide-area) transmission network (over 900 km), covering several islands (i.e., South-Honshu, Shikoku, and Kyushu). The AC transmission lines are used to connect the islands. In addition to the system, it is divided into multiple areas with interconnections (see Fig. 1). Also, an updated capacity of synchronous generators based on each control area is displayed. The power generation and demand are independently operated by six power companies (TSOs) depending on their control schemes [28].

A powerful infrastructure for capturing the necessary simultaneous measurement has been utilized by the WAMS. To examine the inertia of the 60 Hz system, the Japanese WAMS is established via the deployment of distribution-level and transmission-level PMUs (see Fig. 2). The PMU-based time-sequential data are employed to store the measured voltage phasor. In 2019, to study any significant oscillation behavior of the 60 Hz system, four distribution-PMUs were deployed at a domestic supply side throughout four regional Japanese universities (campus WAMS); that is the Kyushu Institute of Technology (μPMU1), Hiroshima University (μPMU2), Osaka University (μPMU3), and Nagoya Institute of Technology (μPMU4). In 2020, to provide better geographical visibility of the longitudinal transmission system, eight transmission-PMUs have been installed at important substations throughout central prefectures; that is Kagoshima (PMU1), Kumamoto, (PMU2), Fukuoka (PMU3), Hiroshima (PMU4), Hyogo (PMU5), Osaka (PMU6), Gifu, (PMU7), and Shizuoka (PMU8).

TABLE 1. Comparison between μ PMU and PMU for inertia estimation.

Classification	μPMU	PMU
Measurement data	Single-phase voltage, phasor	Three-phase voltage, phasor, current
Voltage level	100 V	220 kV or 500 kV
Dynamic data retained time	33 ms.	16 ms.
Accuracy	Low latency	High latency
Data set	36,000 data	108,000 data
Measurement duration	20 min	30 min

A. PHASOR DATA COLLECTION

Fig. 3 depicts a practical overview of the Japan WAMS for inertia estimation. In the distribution level, see Fig. 3(a), the μPMU uses a commercial device (Toshiba NCT2000 Type-A), which exactly measures instantaneous low-voltage (100 V) at the universities/campuses corresponding to the time stamping of the global positioning system (GPS) [8]. To suitably record the system dynamics, the duration of distribution measurements (μPMU) is used as 2/60 s for 20 min per a data set. Accordingly, the set of phasor data of 36,000 data can be collected for a duration of 20 min.

In the transmission level, see Fig.3(b), the transmission-PMU uses a manufactured device, which precisely records three-phase instantaneous high-voltage (220/500 kV) at the substations corresponding to the GPS time stamping [8]. To properly measure the system dynamics, the duration of transmission measurements (PMU) is used as 1/60 s for 30 min per a data set. Consequently, a set of phasor data of 108,000 data can be collected for a duration of 30 min.

By comparing these two-measurement data (see Table. 1), it is obvious that the transmission-PMU data can report measurements with higher accuracy (i.e., high temporal resolution), while the distribution-PMU data have lower accuracy due to a low sampling frequency rate, causing the degraded latency of measurement performance. It should be noted that when performing inertia estimation, the duration of measurement is a sensitive criterion, and a compatibility analysis of these two data types is required. Thus, the appropriate duration of measurement data should be defined based on the evaluation index regarding each PMU type.

In the WAMS condition, a precise pulse per second (PPS) output from the GPS is used to create a synchronized monitoring system. The rapid communication network is used to establish the recorded remote data, creating reliable measurements for specific time. The measured phasor data from μPMUs and transmission-PMUs are automatically obtained via the phasor data concentrator (PDC) and stored via the Internet. The stored data by PDC are transformed into the comma-separated value format for usability. Next, the

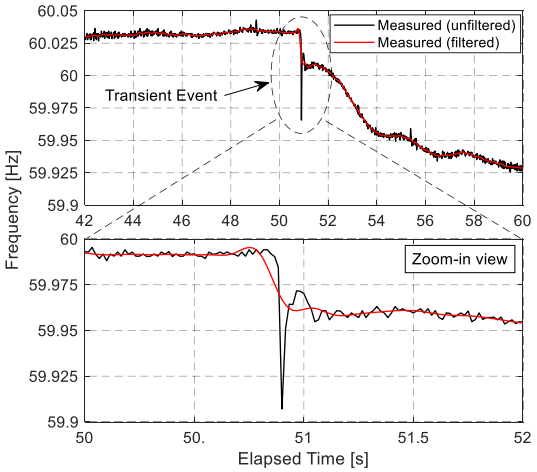

FIGURE 4. Frequency transient filtered by the low-pass band.

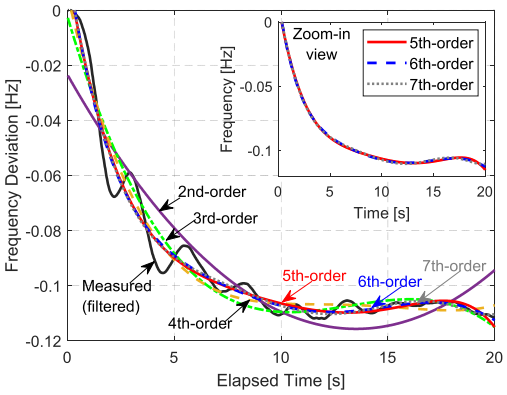

FIGURE 5. The polynomial approximations with the changing number of orders from a first-order to a seventh-order.

modified data are collected via network-attached storage with large capacities at the central equipment (CE). Then, the phasor voltage is calculated using the measured sinusoidal voltage as [8]:

$$\dot{V}\frac{\sqrt{2}}{N}\left(\sum_{k=1}^{N} V_K \sin k\delta_s + j\sum_{k=1}^{N} V_K \cos k\delta_s\right) \quad (4)$$

where δ_s is the sampling angle, N is the voltage sampling number, $\dot{V}$ is the phasor voltage, and V_k is the sequential data of voltage [8].

Finally, the voltage phase (δ) and amplitude (V) can be determined as [8]:

$$\delta = \tan^{-1}(V_{Img}/V_{Re}) \quad (5)$$

$$V = \sqrt{(V_{Re}^2 + V_{Img}^2)} \quad (6)$$

where V_{Re} is the real portion of phasor voltage, and V_{Img} is the imaginary portion of phasor voltage.

B. FREQUENCY AND RoCoF ESTIMATION

The frequency measurement from the 60 Hz system is primarily achieved by the installed PMUs. Although all PMUs are synchronized by the time-stamping at their locations, the PMUs could experience the zero-crossing problem for frequency calculation. Regarding the quantization, the frequency calculation may contain a potential error at specific time, resulting in the poor frequency resolution. To overcome the issue, this work computes the frequency measurement in area j based on the time derivative of voltage phasor as [8], [13]:

$$f_j = f_n + \frac{d\delta_j}{dt}\cdot\frac{f_{pj}}{360} \quad (7)$$

where f_n is the nominal frequency, δ_j is the voltage phasor from PMUs, f_{pj} is the sampling frequency of PMUs, and f_j is the calculated frequency of area j.

Even if the frequency is calculated based on the sample-by-sample in every 33 ms (for μPMUs) or 16 ms (for transmission-PMUs) with high-resolution data, the frequency calculated by (7) might be disturbed by the transient distortions, noises, and measurement errors. To attenuate the dominant characteristic of initial frequency response, the calculated frequency is filtered by a low-pass filter with cutoff frequency around 0.5 Hz. Fig. 4 depicts that the applied filter successfully attenuated the measurement errors, noises, and transient distortions.

Later, the RoCoF (df_j/dt) is computed based on the related time interval between the onset of the primary/initial response and the start of the disturbance. Following the significant disturbance, the initial response of the 60 Hz system can be extracted from 500 ms to 1000 ms. This interval could offer the free-fall of frequency deviation before the mechanism of frequency response is initiated. Hence, the inertia of the 60 Hz system can be estimated by the synchrophasor measurement as a proportional term between the RoCoF and ΔP_j, which equals the M_j-based swing equation [6].

IV. INERTIA ESTIMATION FROM CURRENT JAPANESE WAMS CONSIDERING OSCILLATORY COMPONENTS

The measurement data obtained from PMUs include oscillatory components associated with local oscillations, inter-area (low-frequency) oscillations, and noises [8]. In this section, a polynomial approximation with respect to time is implemented to the measured PMU signal (i.e., frequency) for enhancing the accurate latency of inertia estimation. During the transient/disturbance events, the introduction of a polynomial approximation could effectively restrain the dynamic influence of large oscillatory components (e.g., local oscillation, interarea oscillation), leading to the reduction of estimation errors [12]. Normally, the oscillatory components involve all generators of the system. They represent a phenomenon wherein the oscillation continues for a relatively long period of time, which can threaten system stability. To overcome the challenge, the polynomial approximation is evaluated based on the information on synchronizing power between the generators.

By estimating system inertia using (3), the measured frequency from PMUs may include the oscillatory components driven by synchronizing power between the generators. This

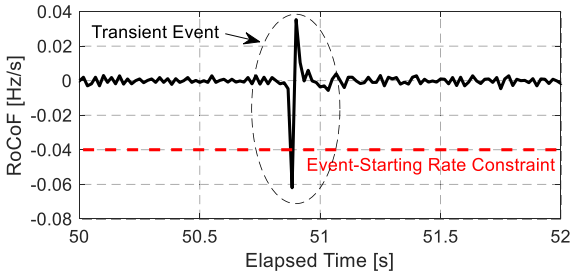

FIGURE 6. **The transient waveform of RoCoF for activating the event-starting time.**

effect would significantly cause the inaccurate RoCoF calculation. This problem would be exacerbated in a longitudinal transmission system. Properly, it is important to accommodate the effect of oscillatory components, avoiding inaccurate inertia estimation. To overcome such a problem, this work applies the polynomial approximation technique to a measured frequency signal of each PMU in an adequate period that prevails large oscillatory components. According to [12], a suitable period where transient events should be recorded is about 15-20 s after the event-starting time.

Focusing on the suitable order of the polynomial approximation, the fifth-order has been used in this work to suppress the influence of large oscillatory components. From Fig. 5, various polynomial approximations with the changing number of orders from a first-order to a seventh-order are presented. By observing the current oscillatory behavior of the 60 Hz system, the fifth-order, sixth-order, and seventh-order yield the most stable waveform with similar characteristics, which can signify remarkable approximation of frequency changes with the lowest disturbance effect. However, applying for a higher-order (over the fifth-order) could cause the complexity of computation. Therefore, the fifth-order approximation is chosen as a sufficient margin for minimizing the estimation error. The frequency change in area j could be defined by the fifth-order polynomial approximation as [12]:

$$\Delta f_j/f_{sj} = A_{5j}t^5 + A_{4j}t^4 + A_{3j}t^3 + A_{2j}t^2 + A_{1j}t \qquad (8)$$

where Δf_j is the frequency change, A_{1j} is the first order coefficient, A_{2j} is the second-order coefficient, A_{3j} is the third-order coefficient, A_{4j} is the fourth-order coefficient, A_{5j} is the fifth-order coefficient, and t is the elapsed time from a start of an event,

By solving the coefficients (i.e., A_{1j} to A_{5j}), the inertia estimation formula regarding the swing equation is defined subject to the polynomial approximation as [12]:

$$\omega_j M_j = \frac{\Delta P_j}{|A_{1j}|} \qquad (9)$$

$$M_j = \frac{\Delta P_j}{2\pi f_{sj}\,|A_{1j}|} \qquad (10)$$

Later, an identification process of event-starting time is explained. In this method, a low-pass filter with cutoff

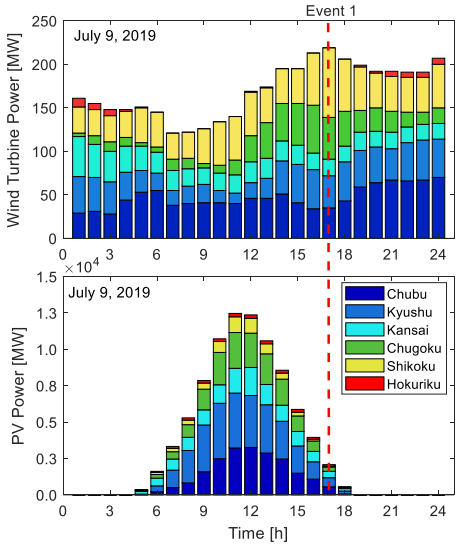

FIGURE 7. **Overview of the existing RES penetration during Event 1.**

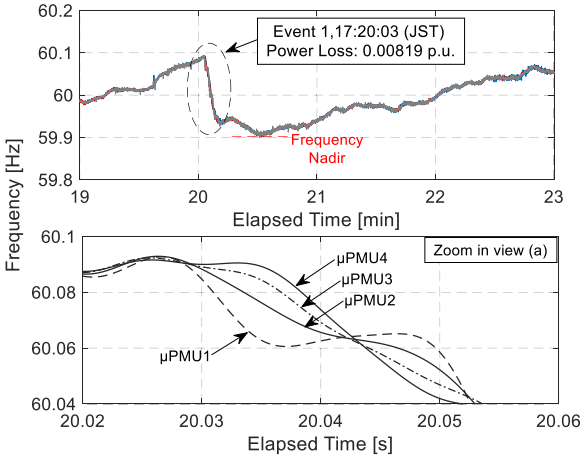

FIGURE 8. **Filtered system frequency response recorded by μPMUs during the western generation trip.**

frequency of 0.5 Hz is also implemented to attenuate the effect of noises and distortions from the measured frequency of each PMU (see Fig. 4). During the transient event (see Fig. 6), the RoCoF constraint is set as 0.04 Hz/s to identify/activate the event-starting time. Subsequently, the frequency change (Δf) can be determined by the fifth-order polynomial approximation for 20 s from the event-starting time.

Lastly, the least-square technique, which is a standard approach in regression analysis, has been used to properly determine the polynomial coefficients (i.e., A_1 to A_5). As described in (10), the system inertia can be successfully estimated by the synchrophasor measurement as a proportional term between the A_{1j} and ΔP_j, equals the M_j.

V. RESULTS OF INERTIA ESTIMATION FROM CURRENT JAPANESE WAMS

In this section, the efficiency and robustness of the polynomial-based inertia estimation and conventional RoCoF-based inertia estimation [16] have been verified by

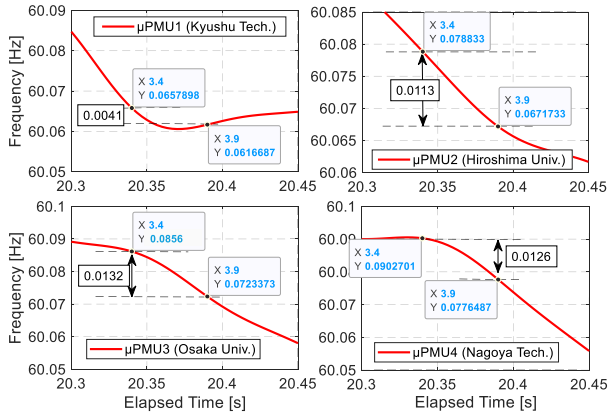

FIGURE 9. RoCoF calculation (500 ms) by μPMUs during the western power loss.

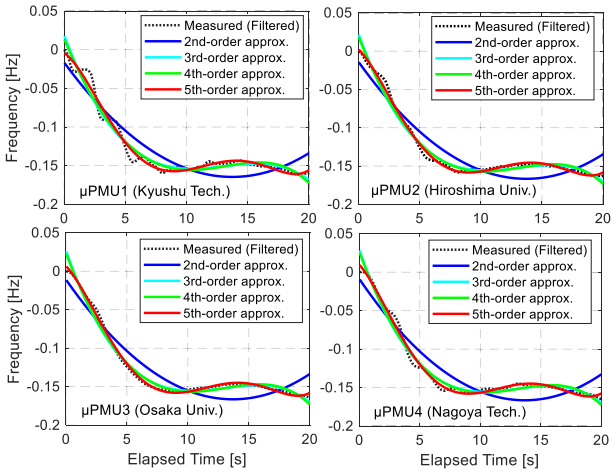

FIGURE 10. Polynomial approximation (20 s) by μPMUs during the western power loss.

real system events from Japanese TSOs regarding different disturbance sizes, disturbance locations, PMU types, and PMU locations.

A. GENERATION LOSS IN THE WESTERN REGION

In the first event (Event 1), the inertia results are estimated based on actual generation loss that occurred at 17:20:03 (JST) of July 9, 2019, in the western region. The size of generation loss (ΔP) was about 0.00819 p.u. of the entire generated power. In addition to the corresponding disturbance size, the data are measured at substations or switching stations of the 500 kV system and provided by Japanese TSOs. The change in inertia energy trigged by the power loss (ΔM) was about 0.0017 p.u. of the entire generated power. The system load was about 0.957 p.u. of the entire generated power. At the time of the disturbance, the whole RES penetration power was about 0.036 p.u. (≈2,296 MW), see Fig. 7 [29]–[34], and system frequency (f_s) was 60.09 Hz. In this scenario, it is also noted that the WAMS observability was only limited to the μPMUs (campus WAMS). The transmission-PMUs (TSO-WAMS) have not yet been installed.

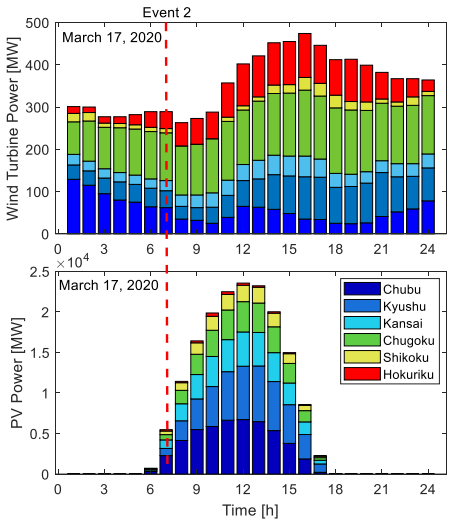

FIGURE 11. Overview of the existing RES penetration during Event 2.

Fig. 8 shows the system frequency responses during the significant generation trip in the western region. At 17:20:03 (JST), the tremendous frequency drop caused by the loss of 0.00819 p.u. could be detected by all μPMUs with the impact decreasing along the path. Within 25 s, the frequency failed to the nadir of about 59.90 Hz. The largest frequency drop for this event was about 200 mHz. The first PMU to detect the event was the μPMU1 in the western region. Its frequency slope after the first drop provides a good indication that the loss origin was in the Kyushu Island and spread from there. After the activation of frequency response services by TSOs, the system frequency took about 120 s to restore to its pre-event value.

Considering the conventional inertia estimation, the corresponding RoCoF quantities regarding individual μPMUs have been computed over 500 ms after the disturbance (see Fig. 9). The starting time is defined as 20.4 s, while the stopping time is defined as 20.9 s. Obviously, different μPMU locations cause discrepancies in the RoCoF calculation. The μPMU1, which is located close to the generation trip entails the lowest RoCoF value. Conventionally, the inertia of the 60 Hz system can be calculated based on the corresponding RoCoF from each μPMU together with the known sizes of ΔP, and ΔM (provided by TSOs), see Table 2. As a result, it is found that the μPMU1, which is situated close to the origin of power loss, estimates the highest inertia value due to the strong influence of oscillatory components. The oscillatory effect is attenuated when the far-away μPMUs (μPMU2, μPMU3, and μPMU4) are used to estimate system inertia, resulting in more realistic estimation. Without considering an effective method to arrest the characteristic of oscillatory components, a huge estimation error could be occurred, causing inaccurate inertia estimation.

To effectively eliminate the influence of large oscillatory components, the polynomial-based inertia estimation is applied to calculate the frequency change from all μPMUs. Then, the calculated frequency changes are used to determine

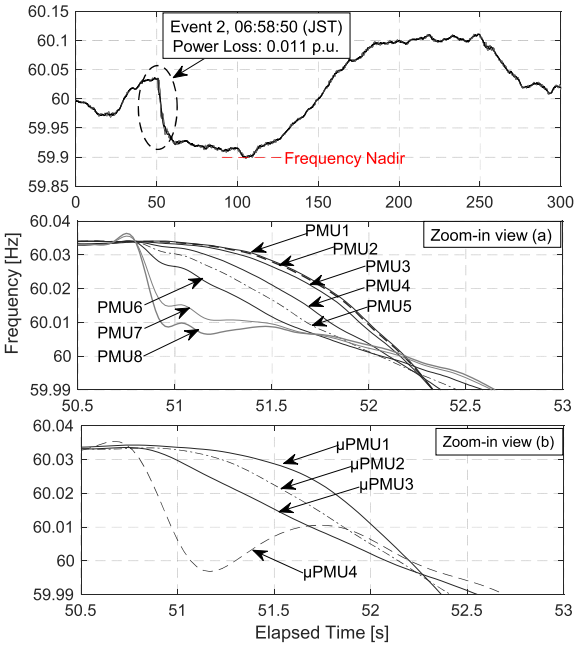

FIGURE 12. Filtered system frequency response recorded by μPMUs and transmission-PMUs during the eastern generation trip.

the first-order coefficient (A_1) for improving the better performance of inertia estimation. Accordingly, the estimated inertia results are successfully improved by (10) with respect to the known size of ΔP, and coefficient A_1. Fig. 10 displays the measured frequency changes based on μPMUs over polynomial approximations with the changing number of orders. By observing the original frequency (see the dashed line) without order approximation, the strong oscillation could be observed due to the high influence of oscillatory components. The strongest oscillation is found at the μPMU1, which is the closest location to the loss event. By increasing the order numbers until reaching the fifth-order, the frequency oscillations from all μPMUs significantly diminish even in the case of the μPMU1 (i.e., the disturbance source). Under the fifth-order approximation, the frequency measurements from all μPMUs have almost the same response. This result signifies that all oscillatory components are effectively diminished, and the fifth-order signal can be reliably used to evaluate the frequency change with respect to the A_1 calculation. Finally, the system inertia quantities are properly calculated based on the measurement of μPMUs as a proportional term between the corresponding A_1 and the known size of ΔP (see Table 2). Using the polynomial method, it is obvious that the estimated inertia quantities from all μPMUs do not significantly change even if the measurement is obtained from the μPMU closest to the disturbance origin.

B. GENERATION LOSS IN THE EASTERN REGION

In the second event (Event 2), the inertia results have been estimated from real generation loss that occurred at 06:58:50 (JST) on March 17, 2020, in the eastern region. The ΔP was about 0.011 p.u. of the entire generated power. In addition to the corresponding disturbance size, the data are measured at substations or switching stations of the 500 kV system and provided by Japanese TSOs. The ΔM was about 0.117 p.u. of the entire generated power. The system load was about 0.927 p.u. of the entire generated power. At the time of the disturbance, the whole RES penetration power was about 0.092 p.u. or (≈5,764 MW), see Fig. 11 [29]–[34], and f_s was 60.035 Hz. This event is mainly recorded by eight transmission-PMUs from the TSO-WAMS. To provide further observability of the event, the measurement data of four μPMUs from the campus WAMS are also analyzed.

Fig. 12 displays the system frequency responses from the large generation trip in the eastern region, which are captured by the transmission-PMUs with extra inclusion of μPMUs. Clearly, a good coincidence of frequency oscillation could be observed by both levels of PMUs. The significant power loss of 0.011 p.u. caused the largest frequency drop of about 140 mHz with its nadir of about 59.90 Hz. A closer inspection of Fig.12 shows that the origin of the event is situated in the eastern region between the μPMU4 and PMU8. To avoid system instability, TSOs activated the frequency response services, and system frequency returned to its nominal value within 50 s. Compared with the previous event, this event results in a smaller size of the frequency drop, which could indicate higher inertia property.

As shown in Fig. 13, the RoCoF values are calculated by both μPMUs and transmission-PMUs over 500 ms after the disturbance. The starting time is used as 51.0 s, and the stopping time is used as 51.5 s. Depending on the individual PMU locations, the corresponding RoCoF values could be computed. The RoCoF calculations from the middle region (i.e., PMU4, PMU5, PMU6, μPMU2, and μPMU3) dictate a higher quantity. On the other hand, the RoCoF calculations from the both-ends of the system yield a lower quantity. Obviously, the PMUs located close to the loss origin (i.e., μPMU4 and PMU8) contain a strong oscillating effect, signifying low RoCoF values. Using the conventional method, the system inertia can be proportionally determined based on the corresponding RoCoF from μPMUs and transmission-PMUs together with the known sizes of ΔP, ΔM, as shown in Table 3. Apparently, the PMUs situated around the both-end provide a higher inertia value due to the lower RoCoF extraction. The PMUs located in the middle part estimate a lower inertia value due to the higher RoCoF extraction. Using the conventional method, the inertia calculated from each PMU location becomes quite variable, indicating the poor RoCoF calculation. This is because the influence of oscillatory components is not effectively arrested, causing difficulty in extracting the initial frequency response. Consequently, it results in a significant inertia estimation error. The second scenario also ensures that the accuracy of the conventional method is highly dependent on the RoCoF calculation with respect to PMU locations. This factor is vastly affected by the oscillatory components. If the RoCoF calculation is not accurate, the conventional method will likely estimate the system inertia with tremendous errors.

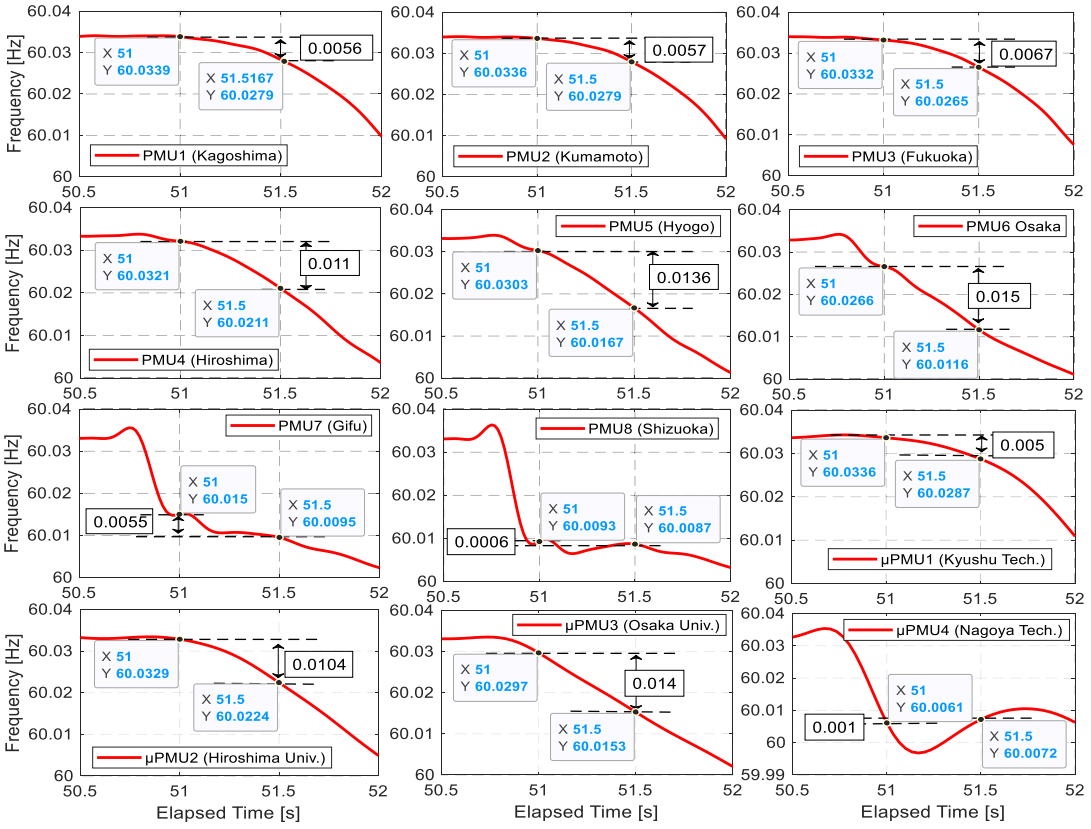

FIGURE 13. RoCoF calculation (500 ms) by μPMUs and transmission-PMUs during the eastern generation trip.

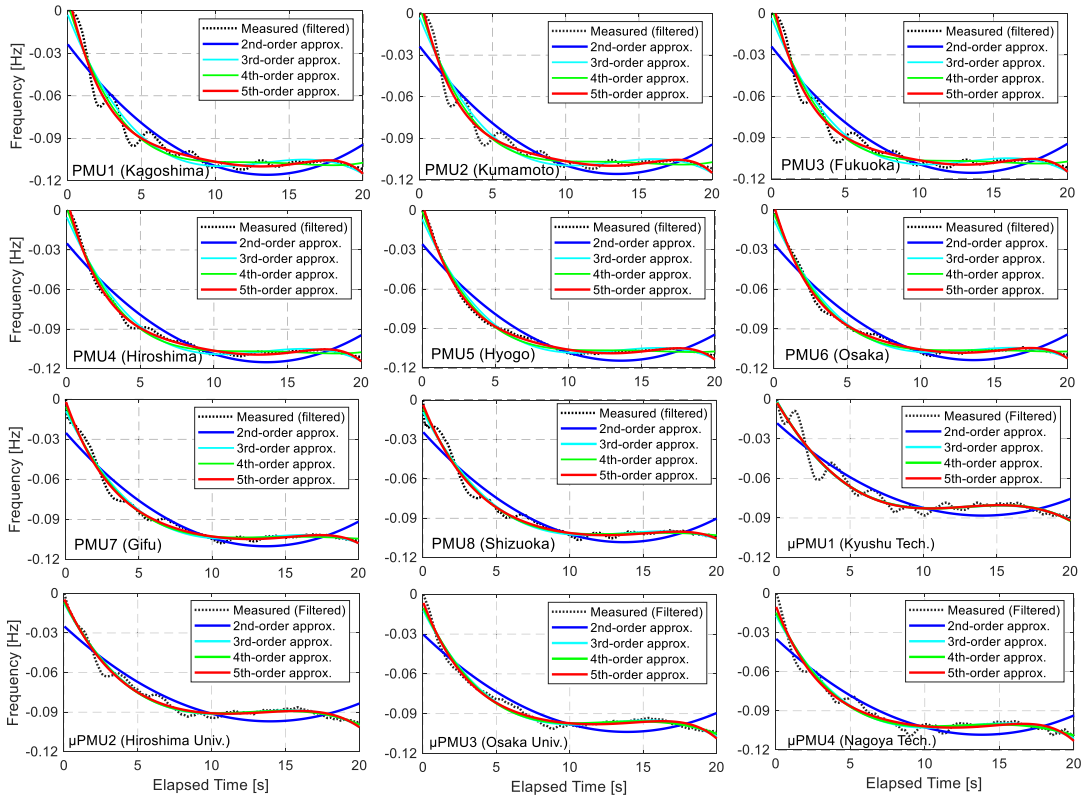

FIGURE 14. Polynomial approximation (20 s) by μPMUs and transmission-PMUs during the eastern generation trip.

TABLE 2. Inertia estimation regarding generation loss on the western region (Event 1).

Location (area/prefecture)	Conventional inertia estimation-based RoCoF			Inertia estimation-based polynomial approximation		
	RoCoF (Hz/s)	M (s)	H (s)	A_1 (x10^{-4})	M (s)	H (s)
μPMU 1 (Kyushu Tech.)	0.00824	59.802	29.901	3.567	23.03	11.515
μPMU 2 (Hiroshima Univ.)	0.02271	21.694	10.847	5.185	15.842	7.921
μPMU 3 (Osaka Univ.)	0.02632	18.582	9.291	5.695	14.424	7.128
μPMU 4 (Nagoya Tech.)	0.02524	19.526	9.763	6.028	13.626	6.813

TABLE 3. Inertia estimation regarding generation loss on the eastern region (Event 2).

Location (area/prefecture)	Conventional inertia estimation-based RoCoF			Inertia estimation-based polynomial approximation		
	RoCoF (Hz/s)	M (s)	H (s)	A_1 (x10^{-4})	M (s)	H (s)
PMU 1 (Kagoshima)	0.0112	58.718	29.359	7.7798	14.031	7.015
PMU 2 (Kumamoto)	0.0114	57.690	28.845	7.7756	14.108	7.054
PMU 3 (Fukuoka)	0.0134	49.097	24.548	7.6086	14.380	7.190
PMU 4 (Hiroshima)	0.022	29.950	14.975	7.1518	15.301	7.651
PMU 5 (Hyogo)	0.0272	24.247	12.123	6.7244	16.272	8.136
PMU 6 (Osaka)	0.031	21.994	10.997	6.1958	17.660	8.830
PMU 7 (Gifu)	0.011	59.783	29.891	5.1951	21.062	10.531
PMU 8 (Shizuoka)	0.0012	547.059	273.529	4.7247	22.314	11.157
μPMU 1 (Kyushu Tech.)	0.010	65.77	32.885	7.8171	13.997	6.9989
μPMU 2 (Hiroshima Univ.)	0.0208	31.68	15.840	7.3851	14.816	7.4083
μPMU 3 (Osaka Univ.)	0.0286	23.072	11.786	6.3889	17.127	8.5635
μPMU 4 (Nagoya Tech.)	0.0002	298.54	149.27	5.1364	21.302	10.651

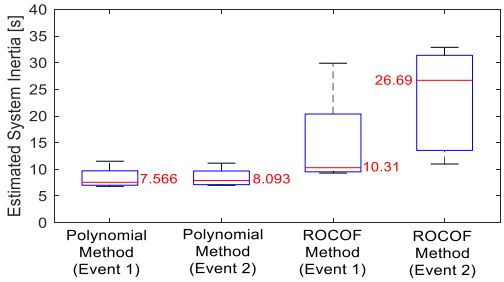

FIGURE 15. Statistical comparison of estimated inertia-based polynomial approximation and conventional RoCoF methods.

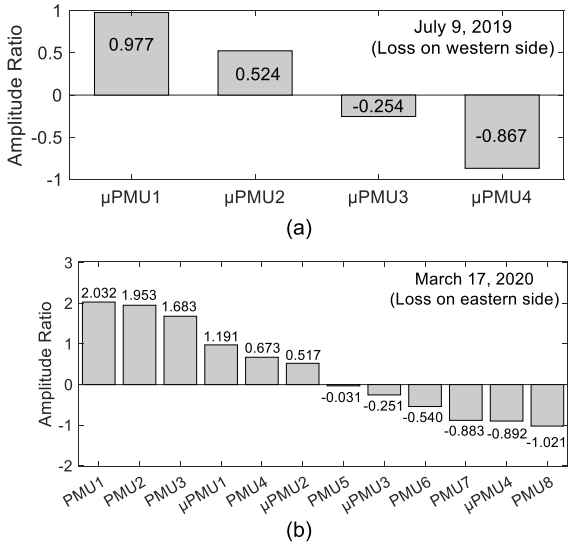

FIGURE 16. Mode shapes associated with PMU locations: (a) Event 1; (b) Event 2.

By applying the polynomial technique, the oscillation effect is significantly eliminated by increasing the order numbers for both PMU levels regardless of their locations (see Fig.14). Clearly, the fifth-order approximation successfully removes the prominent/undesirable oscillations and entails the smoothest frequency response. Accordingly, the frequency change with respect to the A_1 calculation (i.e., the lowest oscillatory and disturbanceeffects) could be properly determined. Finally, the system inertia values from all PMUs are calculated based on the proportional term between the corresponding A_1 and the known size of ΔP as shown in Table 3. Using the polynomial method, the estimated inertia from all PMUs does not substantially variate at the both-ends of the system. It is obvious that the polynomial method could estimate the reliable system inertia with a low variation range for both PMU levels regardless of their locations. Compared with the conventional method, the polynomial method potentially minimizes the inertia estimation error as its modeling does not deal with the direct RoCoF calculation, leading to the improvement of estimation latency.

As shown in Fig.15, the utilization of the statistical analysis confirms the superior performance of the polynomial method. Apparently, the polynomial approximation method could manage to retain a low median for all test events. In addition, the results based on the polynomial approximation did not present a significant increase in estimation errors. On the contrary, the results based on conventional RoCoF estimation demonstrate a higher median for all scenarios. Significantly, the upward trend with the increasing ranges of estimation errors could be observed. Based on this comparison, it is concluded that the polynomial method provides better inertia estimation with a low error range regardless of PMU

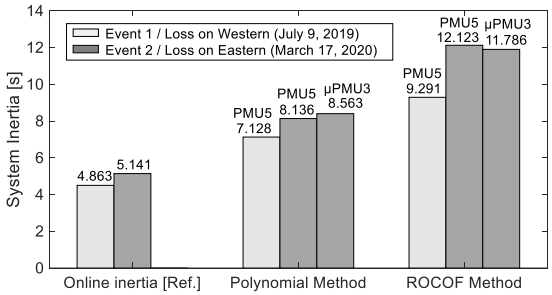

FIGURE 17. Inertia estimation from the potential PMUs.

types, PMU locations, disturbance sizes, and disturbance locations.

Considering the estimation performance on different PMU sites in the longitudinal system, the following section will perform the practical technique to properly evaluate the most effective location for accurate inertia estimation.

VI. DETERMINATION OF SUFFICIENT PMU LOCATION FOR ACCURATE INERTIA ESTIMATION

In real practice, the longitudinal configuration of the 60 Hz Japanese system (i.e., multi-areas of generations) contains the interarea (low-frequency) oscillations, which are dominant in the whole system. The dominant oscillation modes (i.e., a range from 0.2 Hz to 0.8 Hz) have poor damping characteristics, which can put the system in unstable conditions and cause the degradation in inertia estimation performance with errors throughout PMU locations. To determine an effective location for improving the estimation performance, the characteristics of the dominant oscillation mode should be analyzed by all PMU sites in the system. After obtaining the lowest dominant effect, a potential PMU location can represent the COI frequency, which can be practically used for superiority in estimation with high accuracy. Thus, in this section, the comprehensive mode shape analysis is used to evaluate the effective PMU location-based inertia estimation considering the existing interarea oscillation effect.

By considering an amplitude ratio of the dominant oscillation with respect tothe locations of μPMUs and transmission-PMUs, the interarea oscillation characteristics could be effectively analyzed by the mode shape analysis regarding all system events (see Fig. 16). The locations of μPMU3 and PMU5 exhibit the lowest oscillation amplitude for Event 1 and Event 2, respectively. Moreover, the most potential location for estimating inertia with the highest accuracy could be found at the PMU5 (Hyogo), which represents the lowest oscillation amplitude for all system events. The measured frequency from this location can represent the COI frequency, where the lowest impact of interarea oscillations exists. Other locations are vastly affected by the dominant interarea oscillations, resulting in high sensitivity to estimation errors. For the longitudinal system, this analysis also validates that not all PMUs could offer consistent inertia estimation at their locations owing to the relevant response of interarea oscillation. The certain PMU situated in the COI frequency could only estimate the system inertia with accurate latency.

As the huge ongoing substitution of spinning generators by RESs in the 60 Hz system, at the time of the study, it should be remarked that there was no inertia reference with precise accuracy applicable for comparison. The best inertia reference could be obtained only from available online spinning generators (i.e., a sum of all connected generators operated by six power companies) in the system [27]. Hence, the result of the polynomial method is compared with the results of the conventional inertia estimation-based RoCoF and the known contribution of measurable inertia from online generators (see Fig. 17). It is obvious that the estimation error drops about 20% for Event 1 and about 30% for Event 2 when the polynomial method is applied with the potential PMU location. Compared to the measurable inertia from online generation, it is obvious that the polynomial technique could estimate the system inertia closer to the measurable value, indicating the improvement of inertia estimation performance. However, it is noticed that the estimated inertia is still larger than the measurable inertia. This is because the calculation of measurable inertia did not contain the inertia contribution from private/off-line generators (operated by industrialized factories) and induction motors (operated by demand sides), resulting in the difference. Accordingly, the system inertia can be evaluated with the high accuracy when applying the polynomial method in combination with the sufficient PMU-based COI in the longitudinally interconnected system.

VII. CONCLUSION

Throughout the substantial RESs integration, this paper evaluates the inertia of the 60 Hz Japanese power system from transient measurements considering the dynamic effect of changing PMU types and locations with respect to various disturbance sizes and locations. The performance and efficiency of inertia estimation techniques are validated through the real system measurement data. The estimated results from the conventional method contain large estimation errors because the measurement data include multiple oscillation modes. It is obvious that the polynomial method could offer the reliable inertia estimation with a low error range regardless of PMU types, PMU locations, disturbance sizes, and disturbance locations. As a result, it is evident that the recent inertia of the 60 Hz Japanese power system with substantial RESs penetration varies around 7.12 - 8.13 s in the system load base. Also, the significant factor when choosing a sufficient PMU site for estimating inertia with high accuracy relies on the dominant effect of interarea frequency oscillation. The Hyogo area (i.e., PMU 5) is considered as the most effective PMU-based COI location, where the lowest influence of interarea modes occurs. In addition, the refined inertia estimation from the PMU-based polynomial approximation leads to further enhancements of operation, control, and management of the system, offering the robustness against unforeseen transient events caused by substantial RESs penetration.

Further developments of this research would desire to include a study of the range of recorded disturbances that will allow the analysis of precise inertia estimation corresponding to the changing scales of RESs penetration.

ACKNOWLEDGMENT

The authors would like to thank the innovative feedback from the editor of IEEE Access and anonymous reviewers.

REFERENCES

[1] C. Phurailatpam, Z. H. Rather, B. Bahrani, and S. Doolla, "Measurement-based estimation of inertia in AC microgrids," *IEEE Trans. Sustain. Energy*, vol. 11, no. 3, pp. 1975–1984, Jul. 2020.
[2] R. K. Panda, A. Mohapatra, and S. C. Srivastava, "Online estimation of system inertia in a power network utilizing synchrophasor measurements," *IEEE Trans. Power Syst.*, vol. 35, no. 4, pp. 3122–3132, Jul. 2020.
[3] H. Gu, R. Yan, and T. K. Saha, "Minimum synchronous inertia requirement of renewable power systems," *IEEE Trans. Power Syst.*, vol. 33, no. 2, pp. 1533–1543, Mar. 2018.
[4] T. Kerdphol, Y. Matsukawa, M. Watanabe, and Y. Mitani, "Application of PMUs to monitor large-scale PV penetration infeed on frequency of 60 Hz Japan power system: A case study from Kyushu Island," *Electr. Power Syst. Res.*, vol. 185, no. 1, Aug. 2020, Art. no. 106393.
[5] H. Golpira, A. Atarodi, S. Amini, A. R. Messina, B. Francois, and H. Bevrani, "Optimal energy storage system-based virtual inertia placement: A frequency stability point of view," *IEEE Trans. Power Syst.*, vol. 35, no. 6, pp. 4824–4835, Nov. 2020.
[6] K. Tuttelberg, J. Kilter, D. Wilson, and K. Uhlen, "Estimation of power system inertia from ambient wide area measurements," *IEEE Trans. Power Syst.*, vol. 33, no. 6, pp. 7249–7257, Nov. 2018.
[7] U. Akram, N. Mithulananthan, M. Q. Raza, R. Shah, and F. Milano, "RoCoF restrictive planning framework and wind speed forecast informed operation strategy of energy storage system," *IEEE Trans. Power Syst.*, vol. 36, no. 1, pp. 224–234, Jan. 2021.
[8] H. Bevrani, M. Watanabe, and Y. Mitani, *Power System Monitoring and Control*. Hoboken, NJ, USA: Wiley, 2014.
[9] M. Sun, Y. Feng, P. Wall, S. Azizi, J. Yu, and V. Terzija, "On-line power system inertia calculation using wide area measurements," *Int. J. Electr. Power Energy Syst.*, vol. 109, pp. 325–331, Jul. 2019.
[10] M. Kuivaniemi and and, "Estimation of system inertia in the Nordic power system using measured frequency disturbances," in *Proc. CIGRE Conf.*, Lund, Sweden, 2015, pp. 1–6.
[11] D. P. Chassin, Z. Huang, M. K. Donnelly, C. Hassler, E. Ramirez, and C. Ray, "Estimation of WECC system inertia using observed frequency transients," *IEEE Trans. Power Syst.*, vol. 20, no. 2, pp. 1190–1192, May 2005.
[12] T. Inoue, H. Taniguchi, Y. Ikeguchi, and K. Yoshida, "Estimation of power system inertia constant and capacity of spinning-reserve support generators using measured frequency transients," *IEEE Trans. Power Syst.*, vol. 12, no. 1, pp. 136–143, Feb. 1997.
[13] P. M. Ashton, C. S. Saunders, G. A. Taylor, A. M. Carter, and M. E. Bradley, "Inertia estimation of the GB power system using synchrophasor measurements," *IEEE Trans. Power Syst.*, vol. 30, no. 2, pp. 701–709, Mar. 2015.
[14] M. AbolhasaniJabali and M. H. Kazemi, "Estimation of inertia constant of Iran power grid using the largest simulation model and PMU data," in *Proc. 24th Iranian Conf. Electr. Eng. (ICEE)*, Shiraz, Iran, May 2016, pp. 158–160.
[15] A. Fernández-Guillamón, A. Vigueras-Rodríguez, and Á. Molina-García, "Analysis of power system inertia estimation in high wind power plant integration scenarios," *IET Renew. Power Gener.*, vol. 13, no. 15, pp. 1–10, 2019.
[16] T. Kerdphol, M. Watanabe, R. Nishikawa, T. Tamaki, and Y. Mitani, "Determining inertia of 60 Hz Japan power system using PMUs from power loss event," in *Proc. IEEE Texas Power Energy Conf. (TPEC)*, College Station, TX, USA, Feb. 2021, pp. 1–5.
[17] P. Wall, F. Gonzalez-Longatt, and V. Terzija, "Estimation of generator inertia available during a disturbance," in *Proc. IEEE Power Energy Soc. Gen. Meeting*, San Diego, CA, USA, Jul. 2012, pp. 1–5.
[18] X. Cao, B. Stephen, I. F. Abdulhadi, C. D. Booth, and G. M. Burt, "Switching Markov Gaussian models for dynamic power system inertia estimation," *IEEE Trans. Power Syst.*, vol. 31, no. 5, pp. 3394–3403, Sep. 2016.
[19] D. Zografos, M. Ghandhari, and R. Eriksson, "Power system inertia estimation: Utilization of frequency and voltage response after a disturbance," *Electr. Power Syst. Res.*, vol. 161, pp. 52–60, Aug. 2018.
[20] A. Schmitt and B. Lee, "Steady-state inertia estimation using a neural network approach with modal information," in *Proc. IEEE Power Energy Soc. Gen. Meeting*, Chicago, IL, USA, Jul. 2017, pp. 1–5.
[21] F. Zeng, J. Zhang, Y. Zhou, and S. Qu, "Online identification of inertia distribution in normal operating power system," *IEEE Trans. Power Syst.*, vol. 35, no. 4, pp. 3301–3304, Jul. 2020.
[22] T. Kerdphol, M. Watanabe, R. Nishikawa, Y. Hayashi, and Y. Mitani, "Inertia estimation of the 60 Hz Japanese power system from synchrophasor measurements," *IEEE Trans. Power Syst.*, early access, Apr. 19, 2022, doi: 10.1109/TPWRS.2022.3168037.
[23] D. Yang, B. Wang, J. Ma, Z. Chen, G. Cai, Z. Sun, and L. Wang, "Ambient-data-driven modal-identification-based approach to estimate the inertia of an interconnected power system," *IEEE Access*, vol. 8, pp. 118799–118807, 2020.
[24] D. Zografos and M. Ghandhari, "Power system inertia estimation by approaching load power change after a disturbance," in *Proc. IEEE Power Energy Soc. Gen. Meeting*, Chicago, IL, USA, Jul. 2017, pp. 1–5.
[25] D. Wilson, J. Yu, N. Al-Ashwal, B. Heimisson, and V. Terzija, "Measuring effective area inertia to determine fast-acting frequency response requirements," *Int. J. Electr. Power Energy Syst.*, vol. 113, pp. 1–8, Dec. 2019.
[26] Y.-K. Wu, K. Le, T.-A. Nguyen, and O.-D. Phan, "Estimation of power system inertia using traditional swing equation, polynomial approximation and RV methods," in *Proc. Int. Symp. Comput., Consum. Control (IS3C)*, Taichung City, Taiwan, Nov. 2020, pp. 347–350.
[27] NEDO Business Report (WG1), *Improvement of Inertia Estimation Accuracy by FFT Method*, New Energy and Industrial Technology Development Organization, Tokyo, Japan, 2020, vol. SWG2, nos. 1–5, pp. 1–3.
[28] K. Ogimoto and H. Wani, "Making renewables work: Operational practices and future challenges for renewable energy as a major power source in Japan," *IEEE Power Energy Mag.*, vol. 18, no. 6, pp. 47–63, Nov./Dec. 2020.
[29] Chubu Electric Power Company. (2022). *Area Power Supply and Demand Performance Data*. Aichi, Japan. Accessed: May 23, 2022. [Online]. Available: https://powergrid.chuden.co.jp/denkiyoho/
[30] Hokuriku Electric Power Company. (2022). *Area Supply and Demand Results*. Toyama, Japan. Accessed: May 23, 2022. [Online]. Available: https://www.rikuden.co.jp/nw_jyukyudata/area_jisseki.html
[31] Chugoku Electric Power Company. (2022). *Area Supply and Demand Record*. Hiroshima, Japan. Accessed: May 23, 2022. [Online]. Available: https://www.energia.co.jp/nw/service/retailer/data/area/
[32] Shikoku Electric Power Company. (2022). *Supply and Demand Performance*. Kagawa, Japan. Accessed: May 23, 2022. [Online]. Available: https://www.yonden.co.jp/nw/renewable_energy/data/supply_demand.html
[33] Kansai Electric Power Company. (2022). *Area Supply and Demand Results*. Kansai, Osaka. Accessed: May 23, 2022. [Online]. Available: https://www.kansai-td.co.jp/denkiyoho/area-performance.html
[34] Kyushu Electric Power Company. (2022). *Area Supply and Demand Results*. Fukuoka, Japan. Accessed: May 23, 2022. [Online]. Available: https://www.kyuden.co.jp/td_service_wheeling_rule-document_disclosure

THONGCHART KERDPHOL (Member, IEEE) received the Ph.D. degree in electrical and electronic engineering from the Kyushu Institute of Technology (Kyutech), Japan. From 2016 to 2017, he was a Postdoctoral Fellow with the Electrical and Electronic Engineering Department, Kyutech. From 2018 to 2019, he was a Visiting Researcher/a Lecturer with the Department of Power Mechatronics and Drives, Clausthal University of Technology (TU Clausthal), Germany. He is currently a Research Fellow with the Department of Electrical and Electronic Engineering, Kyutech. He has authored a textbook entitled "*Virtual Inertia Synthesis and Control*" and over 50 journals/conference papers. He is also open to join research opportunities and collaboration with other research groups. His research interests include power system stability, PMUs, robust control, intelligent optimization, and smart/micro-grid control.

MASAYUKI WATANBE (Member, IEEE) received the B.Sc., M.Sc., and D.Eng. degrees in electrical engineering from Osaka University, Japan, in 2001, 2002, and 2004, respectively. Since 2004, he has been with the Department of Electrical and Electronic Engineering, Kyushu Institute of Technology (Kyutech), Fukuoka, Japan, where he is currently working as a Professor. He is the Holder of the PMU Licensed Patent. He has authored numerous books/book chapters and over 200 journals/conference papers. His research interest includes the area of the analysis of power systems.

YASUNORI MITANI (Member, IEEE) received the B.Sc., M.Sc., and D.Eng. degrees in electrical engineering from Osaka University, Japan, in 1981, 1983, and 1986, respectively. From 1994 to 1995, he was a Visiting Research Associate with the University of California at Berkeley, Berkeley (UC Berkeley), USA. From 2016 to 2018, he was the President of the Institute of Electrical Engineers of Japan (IEEJ), Power and Energy Society. He is currently the President of the Kyushu Institute of Technology, Japan. He has authored numerous books/book chapters and over 300 journals/conference papers. His research interests include power system stability, dynamics, and control.

ISSARACHAI NGAMROO (Senior Member, IEEE) received the Ph.D. degree in electrical engineering from Osaka University, Japan, in 2000. He is currently a Professor with the Department of Electrical Engineering, Faculty of Engineering, King Mongkut's Institute of Technology Ladkrabang, Bangkok, Thailand. His research interests include power system stability, dynamic, and control.